ExB probe measurements in the plasma plume of a 100 W-class Hall thruster

T Hallouin, S Mazouffre

E×B probe measurements in the plasma plume of a 100 W-class Hall thruster

SPACE PROPULSION 2020+1

17 - 18 - 19 MARCH 2021

T. Hallouin[1,2,*] and **S. Mazouffre**[2]

[1]*Exotrail, Massy, Essone, 91300, France*
[2]*Centre National de la Recherche Scientifique, Orléans, Loire, 45000, France*
[*]**Email:** thibault.hallouin@cnrs-orleans.fr

March 1, 2021

Keywords

Hall thruster, E×B probe, multiply-charged ions, krypton, xenon

Abstract

The ion far-field plume of the 100 W-class ISCT100-v2 Hall Thruster (HT) has been characterized by means of an **E×B** probe. The influence of operating parameters on both velocities and fraction of different ion species was investigated over a 40° circular arc. **E×B** spectra were thus recorded for different background gas pressures, discharge voltages, angular positions and propellants (namely xenon and krytpon). The probe alignment is also discussed in this contribution, since measurements were recorded for the probe aligned with both the thruster centerline and the thruster mid-channel.

1 Introduction

In Hall thrusters operating at high anode mass flow rates and/or high discharge voltages, a significant fraction of multiply charged ions can be created. Such species degrade the efficiency and the mass utilization of Hall thrusters (HTs) [1]. They also increase erosion and sputtering on spacecraft surfaces, owing to their high momentum and charge state in comparison to singly charged ions [2, 3]. Determining the fraction of ion species as well as their distribution in the plume is thus relevant to provide thrust correction factors and to assess accurately the erosion of the thruster discharge channel. It is also appropriate to gain insight into ionization processes in magnetized plasmas.
To do so, various diagnostic tools have been used to explore ion distribution. Many studies have investigated ion energy using a Retarding Potential Analyzer (RPA) [4, 5, 6] or a Molecular Beam Mass Spectrometer (MBMS) [7, 2]. However the last diagnostic fails in discrimating multiply charged from singly charged ions as the current collected is dependent on the energy per unit charge of the ion species [8]. The second tool is time-consuming with a limited resolution [9].
The **E×B** probe, or Wien filter, has been used in electric propulsion since the 1970s to characterize ions beam of Gridded Ion Engines (GIEs). It is in the late 1990s that the E×B probe has been used to investigate Hall thrusters plume [10]. Since then, the filter has been extensively used to investigate plumes of various Hall Thrusters as exemplified in Table 1. The Table 1 clearly suggests that low-power HT plumes are very under-studied. However, it is well known that low-power HTs exhibit performances below mid- and high-power devices due to a large surface-to-volume ratio. It is therefore of interest to measure small thruster plume properties to verify whether the size also has an impact on plume characteristics. To do so, the far-field plume of a 100 W-class HT has been recently characterized in terms of current density profile, total ion current, and ion energy content (see Refs. 11 and 12). To fully complete plume characterization, **E×B** measurements have been performed and are presented in this contribution.
Ion specie fractions are thus assessed as a function of different operating parameters, i.e. the residual gas pressure, the discharge voltage, the anode mass flow rate, the propellant type. Measurements were also performed for different angles and probe positions, namely, aligned with the thruster axis and aligned with the centerline of the discharge channel.

2 Setup and Instruments

2.1 NExET Vacuum Chamber

E×B measurements have been performed in the NExET—New Experiment on Electric Thrusters—vacuum chamber, a

Table 1: **E×B** probe measurements performed in the plume of various power-class HTs

Hall thrusters	**HT class**	**References**
SPT-100	1.35 kW	Kim & Gallimore [10, 2]
P5	5 kW	Gallimore [2]
NASA-173Mv2	5 kW	Hofer [13, 14]
BHT200-X3	200 W	Ekholm [15]
BHT-HD-600	600 W	Ekholm [16]
H6	6 kW	Reid [17]
Unnamed	500 W	Diamant [18]
BHT-1500	2 kW	Diamant [19]
PPS-1350	1.5 kW	Diamant [20]
Z-70	600 W	Gurciullo [21]
Unnamed	100 W	Watanabe [22]

stainless-steel cylindrical tank 1.8 m in length and 0.8 m in diameter. NExET is fitted with a primary dry pump that evacuates 400 $m^3 \cdot h^{-1}$, and two turbomolecular pumps, with an overall pumping speed of 650 l/s-N_2. A cryogenic panel absorbs heavy-atoms such as xenon and krypton, the two propellants used in this experiment. The pumping speed is around 8000 l/s when the 0.5 m^2 cold panel is sustained at 35 K. The overall pumping system guarantees a background operating pressure below 5×10^{-5} mBar-N_2, proportional to the mass flow rate injected. Note, that since the adsorption temperature of the krytpon is lower than 35K, background pressure for krytpon operation was slightly higher but still below 10^{-4} mBar-N_2.

2.2 100 W-Class ISCT100-v2

The ISCT100-v2, standing for ICARE Small Customizable Thruster, is a 100 W-class Hall thruster (see Figure 1), with performances comparable to the Busek BHT-100 [23]. The ISCT100-v2 corresponds to the $2S_0$-$2B_0$ configuration presented in Ref. 24 and constitutes an example of a low-power Hall thruster. The annular discharge channel is made of BN-SiO_2. A non-magnetic stainless-steel ring anode is placed at the back of the discharge channel, against the internal surface of the outer ceramic wall. The propellant gas is injected homogeneously inside the channel through a mullite disk, of which the high porosity allows for diffusion of the gas. The magnetic field is generated by means of cylindrical samarium-cobalt (Sm-Co) permanent magnets, located on both sides of the annular channel. The symmetrical distribution as well as the lense-shape of the magnetic field are provided by a pure iron magnetic circuit. The maximum magnetic amplitude is reached at the channel exit plane, while a near-zero amplitude is reached in the anode area. Due to the use of permanent magnets, the magnetic field is assumed constant for all operating points which constitutes a large discrepancy with mid- and high- power HTs operation. Indeed, the magnetic field is generated by magnetic coils and varied with operating parameters (i.e. anode mass flow rate and discharge voltage). During these experiments, both high-purity xenon and krypton were used as the propellant gas for the ISCT100v2.

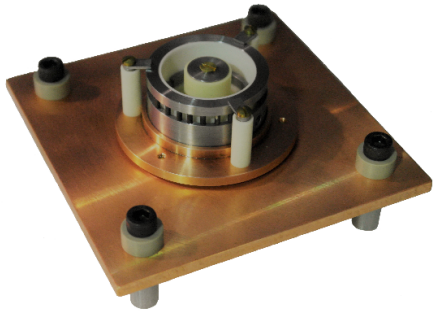

Figure 1: ISCT100-v2, 100 W-class HT.

Table 2: Tested operating points.

U_d **[V]**	P_d **[W]**	$\dot{m}_a$ **[sccm]**
Xenon operation		
200	66	5
250	85	5
300	105	5
350	126	5
Krytpon operation		
250	90	7.2
300	114	7.2

A 1A-class LaB_6 hollow cathode was used to generate the electron current needed for discharge balance and beam neutralization. The cathode orifice is aligned with the thruster centerline and placed at 7.5 cm above the thruster inner pole and 1.5 cm upstream the channel exit plane. The inclination angle is fixed to approximately 45°. The cathode was operated under steady conditions with 2 sccm of Xenon and a constant heating power adapted to maintain a Cathode Reference Potential (CRP) around −10 V.

2.3 Langmuir probe

To accurately assess the actual ion velocity, plasma potential V_p was measured thanks to a cylindrical Langmuir probe in the vicinity of the E×B entrance collimator [21]. The Langmuir probe consists of a 0.38 mm diameter tungsten wire, with a collecting part of 10 mm long. The remaining part is insulated from the surrounded plasma by alumina tubes. The probe axis was oriented parallel to the **E×B** probe axis, at a distance of 3.5 cm from the entrance collimator. The ALP System^{TM} unit from *Impedans Ltd* has been used to acquire the I–V curves. The plasma potential V_p is obtained from the maximum of the first derivative of the I–V curve ($V_p = ((dI)/(dV))_{max}$).

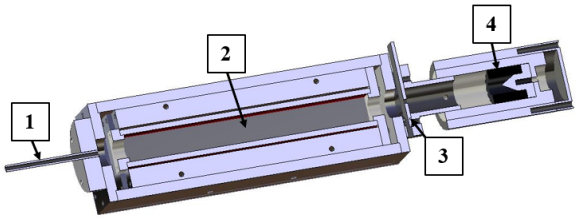

Figure 2: Exploded view of the **E**×**B** probe with the entrance collimator (1), the E×B fields regions (2), the exit collimator (3) and the graphite collector (4).

2.4 E×B probe

2.4.1 Design and theory

E×**B** probe, also known as Wien filter, is a diagnostic tool that allows to measure ion velocity in a given direction [25]. It is therefore essentially used to discern the ion species according to their mass to charge ratio, i.e. the degree of ionizaton of an ion. The working principle of such filter is based on the Lorentz force F_L which represents the deflecting force acting on a charged particule moving at a velocity **u** within an electromagnetic field:

$$\mathbf{F}_L = Ze(\mathbf{E} + \mathbf{u} \times \mathbf{B}) \tag{1}$$

By balancing **E** or **B** intensity, the electromagnetic force acting on the particle can be null, so Equation 1 becomes:

$$\mathbf{E} + \mathbf{u} \times \mathbf{B} = 0 \longrightarrow \mathbf{E} = -\mathbf{u} \times \mathbf{B} = \mathbf{B} \times \mathbf{u} \tag{2}$$

In the case of an **E**×**B** probe, magnetic and electric fields are in crossed field configuration, i.e. $\mathbf{E} \perp \mathbf{B}$. Thus, in a three dimensional Cartesian coordinate system (x,y,z), $\mathbf{E}(0, E_y, 0)$ and $\mathbf{B}(0, 0, B_z)$, so:

$$u_x = \frac{E_y}{B_z} \tag{3}$$

To do so, an **E**×**B** probe is composed of an entrance and an exit collimator, an E×B region and a collector (see Figure 2). In our probe, the magnetic field is constant and generated by $SmCo_5$ permanents magnets spaced of 18 mm. The magnetic flux is distributed homogenously and focused in the axis of the probe thanks to a magnetic steel circuit. The magnetic field at the center of the probe is 1750 G. The electric field is generated by two parallel electrodes separated by a distance d = 16 mm and symmetrically biased.
The entrance collimator is a grounded stainless steel tube with a 2 mm diameter and 55.5 mm long, so that an acceptance angle of 4.13° is achieved. Note that different sets of measurements have been performed with collimators of different dimensions (length and diameter) and materials (quartz, inox). The actual collimator is thus a trade-off between optimal resolution and measurable collector current. The exit collimator is a grounded plate with a 4 mm diameter aperture.
The graphite collector is insulated from the rest of the probe in a Teflon tube. Its conic shape limits the impact of secondary electrons emission due to bombardment of ions.
The voltage between the two electrodes was varied between ± 150 V, with a steap of 0.2 V [25]. One plate was ramped positive and the other was ramped negative with respect to ground, in such a way that the potential at the center of the probe is at ground. The collected current is measured with a Keithley 6485 Picoammeter. It has a range from 20 fA to 20 mA with a resolution of 10 fA.

2.4.2 Probe internal pressure analysis

Particle build-up inside the probe can lead to corrupted results. It is then of interest to evaluate how much time is needed to reach a probe internal pressure for which the corresponding mean free path is similar to the characteristic probe dimensions, i.e. the gap between the electrodes. To do so, a mass continuity analysis was performed to quantify the increase of internal pressure during far-field plume measurements. To simplify the problem, we assume that only ions enters the probe. Thanks to previous Faraday cup measurements performed in the far-field plume of the ISCT100-v2 [12], we consider that the ion current density reaching the entrance collimator of the probe is 0.2 mA/cm^2 at $\theta = 0°$. Thus, for an initial internal pressure of 1×10^{-5} mBar-N_2, it would take more than 1400 hours to reach a probe internal pressure of 5.7×10^{-4} mBar-N_2, corresponding to a mean free path of 16 mm. Such conditions are not achievable in the case of our study. We can thus state that spectra presented in this study are not corrupted by collisions occuring inside the probe.

2.4.3 Spectrum analysis

A typical **E**×**B** spectrum is shown in Figure 3. The measurement was recorded for U_d = 250 V and $\dot{m}_a$ = 5 sccm at 3.6 × 10^{-5} mBar-N_2 background pressure, with the probe aligned with the thruster centerline. The different ion species can be identified as they form different peaks. The main peak corresponds to singly-charged ions Xe^+. Xe^{2+} and Xe^{3+} ion species are also visible at a lower magnitude. One can also notice a low-velocity ion population before the Xe^+ peak. While this extra peak has been reported in other **E**×**B** plume measurements [15, 21, 26], the actual origin still remains unknown. Further investigation will be proposed in this article. Moreover, an overlap area between singly- and doubly-charged particle is visible. It has been identified as the result of elastic collisions between the two entities [2, 10, 27].
To ease the identification of each ion specie, the corresponding probe voltage and velocity are given in Table 3. To verify the reliability of the measurements, we suggest to compare the corresponding velocity v_{ion} to the theoretical value v_{th}. The theoretical value is given by the following Equation:

$$v_{th} = \sqrt{\frac{2eZ(U_d - |CRP|)}{m_{xe}}} \tag{4}$$

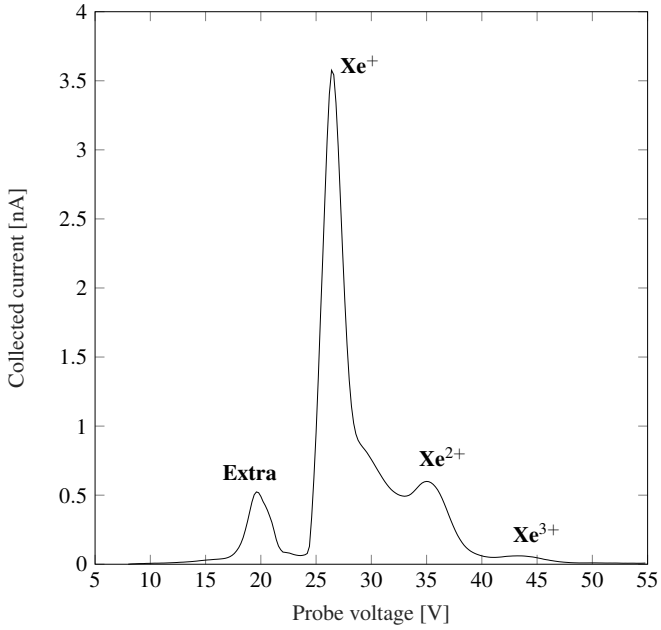

Figure 3: $\mathbf{E}\times\mathbf{B}$ spectrum for $U_d = 250$ V and $\dot{m}_a = 5$ sccm (xe) for $\theta = 0°$, with the probe aligned with the thruster centerline.

Thus, for $U_d = 250V$ and a CRP of -10 V, the theoretical velocities for each ion specie are: $v_{th}(Xe^+)$ = 18.782 km.s^{-1}, $v_{th}(Xe^{2+})$ = 26.482 km.s^{-1}, $v_{th}(Xe^{3+})$ = 32.117 km.s^{-1}. For a specific probe voltage, the corresponding velocity can be determined thanks to the following Equation:

$$v_{ion} = \frac{V_{plates}}{Bd} \tag{5}$$

Since the entrance collimator is grounded, ions face a potential drop that corresponds to the difference between the plasma potential in the vicinity of the probe and the on-axis potential (basically 0V). Therefore, it accelerates ions, causing a shift of the spectrum toward higher velocities. The corrected ion velocity can be determined with the following Equation [21]:

$$v_{ion_c} = \sqrt{v_{ion}^2 - \frac{2eZ(V_p)}{m_{xe}}} \tag{6}$$

For the conditions described above, the plasma potential is 5.3 V. Both measured and corrected ion velocities are given in Table 3. The velocity ratio between $v_{ion_c}(\mathrm{Xe}^{2+})$, respectively $v_{ion_c}(\mathrm{Xe}^{3+})$, and the $v_{ion_c}(\mathrm{Xe}^{+})$ is 1.33, 1.63 respectively. While these ratios are not exactly equal to the theoretical ratios $\sqrt{2}$ and $\sqrt{3}$, ion velocities are still consistent with expected values. Actually, it demonstrates that multiply-charged ions are created in the donwstream region of the discharge chamber since they experience a lower acceleration potential than singly-charged ions.

In addition to a velocity analysis, such spectrum can allow to estimate ion species fraction at a given condition. To do so, we use the method suggested by Hofer [28]. It consists of evaluating the current of each specie as the maximum peak height. Although this method pointed out its limit in terms of accuracy as it does not consider overlap areas and peak width [29, 30], it still constitutes a good approximation to estimate the fraction of ion species. Since the origin and the content of the extra peak is still unclear, it is not considered in the computation of the fractions.

Table 3: Probe voltages and velocities of each ion specie for U_d = 250 V and $\dot{m}_a$ = 5 sccm (Xe), measured on the thruster centerline.

Ion specie	V_{plates} [V]	v_{ion} [km.s^{-1}]	v_{ion_c} [km.s^{-1}]
Extra	19.6	14.000	-
Xe^+	26.4	18.857	18.649
Xe^{2+}	35.2	25.143	24.831
Xe^{3+}	43.2	30.857	30.476

Table 4: Ion species fraction of the ISCT100-v2 for U_d = 250 V and $\dot{m}_a$ = 5 sccm (Xe), measured on the thruster centerline.

Ion specie	Current collected [nA]	Fraction [%]
Xe^+	3.576	0.85
Xe^{2+}	0.598	0.14
Xe^{3+}	0.061	0.01

2.4.4 Experimental set-up and alignment

In the course of this study, both the ISCT100-v2 and the 1A-class cathode were mounted on a Newport URS100BCC motorized rotation stage. The rotation angle θ could be varied between $-20°$ and $20°$ with a step of $5°$, the thruster centerline corresponding to $\theta = 0°$. The $\mathbf{E}\times\mathbf{B}$ probe was mounted on a Newport translation stage, so that the axis of the probe could be aligned either with the thruster axis or with the center of the discharge channel. The probe was aligned thanks to a collimated red laser beam passing through the back of the probe, the entrance collimator and reaching the inner pole of the thruster. Note that the distance R between the entrance aperture of the probe (i.e. the entrance collimator) and the exit plane of the thruster was set at a distance of 34 cm, nearly 10 times the mean discharge channel diameter of the HT.

Measurements were thus recorded for the probe aligned with the thruster centerline and with the thruster mid-channel, respectively. Figures 4a and 4b show the two corresponding spectra obtained under identical thruster operating conditions. Comparatively, the collected current is maximized when the probe is aligned with the thruster centerline, which is consistent with Diamant's observation [18]. Furthermore, one can notice that the width of the signal is larger in the first configuration. Such observations are not surprising. Indeed, when the probe is aligned with the thruster centerline, the field-viewing probe includes the whole annular discharge channel, while in the second configuration, only one side of the discharge channel is probed. The collected ion flux density is logicaly higher

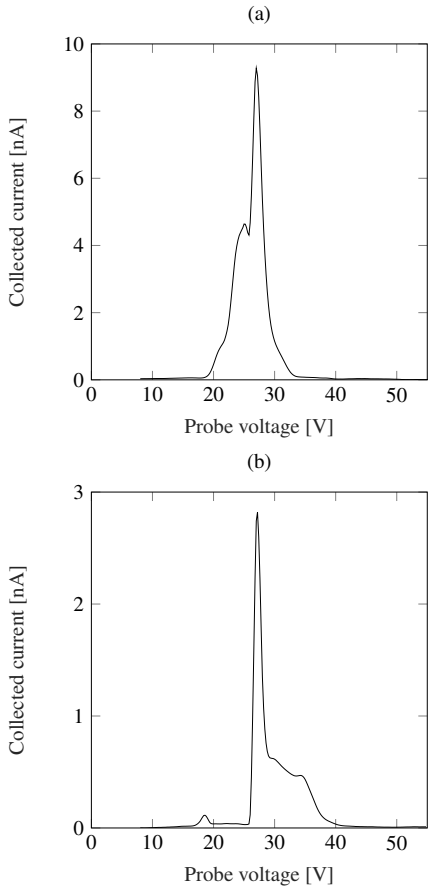

Figure 4: **E**×**B** spectra for U_d = 250 V and $\dot{m}_a$ = 5 sccm for the probe aligned **(a)** with the thruster axis and **(b)** with the channel axis.

in the first configuration. However, while the collected current differs for the two configurations, ion fractions are not impacted by the probe position, as suggested in Table 5. In like manner, the probe voltage (i.e. ion velocity) associated to each peak remains unchanged whatever the probe position. For the sake of clarity, the spectra displayed in the rest of this article correspond to measurements recorded for the **E**×**B** probe aligned with the thruster centerline.

Table 5: Ion species fraction of the ISCT100-v2 for U_d = 250 V and $\dot{m}_a$ = 5 sccm (Xe), for two different probe alignments.

Probe alignment	Xe^+ fraction	Xe^{2+} fraction
Thruster centerline	0.85	0.15
Mid-channel	0.86	0.14

3 Results

3.1 Effect of the background pressure

The effect of background pressure was investigated in this work. The background pressure was artificially increased within the vacuum chamber by directly injecting pure xenon through a Swagelok metering valve. Thus, probe measurements were performed at the operating pressure P_1 (Figure 5a), and two higher background pressures, namely $P_2 = 2P_1$ (Figure 5b) and $P_3 = 3P_1$ (Figure 5c). Measurements were performed for the probe axis aligned with the thruster centerline. From the set of curves, we can observe that the multiply-charged ions fraction increases with background pressure, which is consistent with previous studies performed for mid- and high-power HTs [19, 20]. Ions fractions are presented in Table 6.

Table 6: Ion species fraction recorded for three different background pressure. The ISCT100-v2 was operated with U_d = 250 V and $\dot{m}_a$ = 5 sccm (xe).

Pressure [mBar - N_2]	Xe^+	Xe^{2+}	Xe^{3+}
$P_1 = 3.2 \times 10^{-5}$	89%	11%	0%
$P_2 = 6.5 \times 10^{-5}$	83%	15%	2%
$P_3 = 9.7 \times 10^{-5}$	83%	15%	2%

Furthermore, one can notice that when the background pressure is ramped up, both the extra peak amplitude and the mean equivalent velocity increase, in such a way that it merges with the Xe^+ peak at the highest pressure.

An other interesting feature concerns the overlap between singly- and doubly- charged particle peaks. The overlap decreases when the pressure is ramped up. At high background pressure (Figure 5c), the ion peaks are well defined and well separated.

3.2 Effect of the discharge voltage

The effect of the discharge voltage was also investigated. Measurements were recorded for the probe aligned with the thruster centerline at $\theta = 0°$. The ISCT100-v2 was operated with a xenon mass flow rate of 5 sccm. Measurements were performed for four different discharge voltages, namely 200 V, 250 V, 300 V and 350 V, respectively plotted in Figures 6a, 6b, 6c and 6d. The current collected by the probe increases with discharge voltage, since the ion production is favoured. In like manner, an increase of the discharge voltage causes a shift of the spectra toward higher values of the electrode voltages, that means toward larger velocities. It is nonetheless interesting to note that, compare to what is commonly observed, the multiply-charged ions fractions decrease when the discharge voltage is ramped up, as presented in the Table 7. While this observation differs from other studies [10, 13, 14, 17], it is worth to consider it with caution. Indeed, the observation is made on the thruster centerline at $\theta = 0°$. It is known that at a fixed magnetic field topology, when the discharge voltage is ramped up, the spatial extent of acceleration area increases [31]. Since multiply-charged ions are produced downstream, it is possible that for high discharge voltages, they are directed toward large angles. To be consistent enough, further **E**×**B** measurements must be performed at large angles. Only a complete angular integration would al-

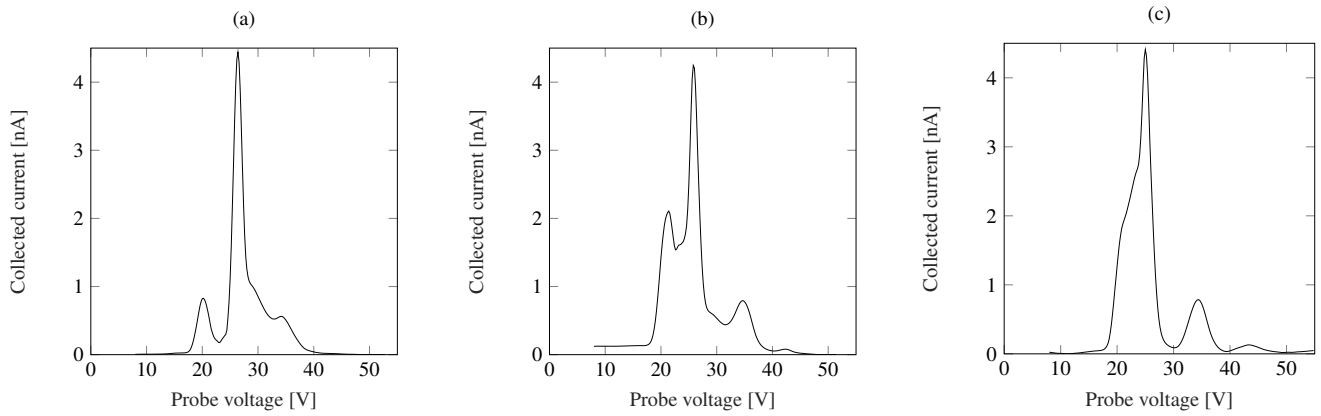

Figure 5: **E**×**B** spectra for U_d = 250 V and $\dot{m}_a$ = 5 sccm at different background pressures, namely **(a)** $P_1 = 3.2 \times 10^{-5}$ mBar-N_2 , **(b)** $P_2 = 6.5 \times 10^{-5}$ mBar-N_2 and **(c)** $P_3 = 9.7 \times 10^{-5}$ mBar-N_2. The measurements were recorded for $\theta = 0°$, with the probe aligned with the thruster axis.

low us to conclude on the fact that multiply-charged ion fractions increase with the discharge voltage. Preliminary angular investigations are discussed in the following section. Other factors might also explain this tendency, namely, the peak-height method used to estimate the ion specie fractions that do not consider the area under the curve, and the extra peak which is not considered in the assessment of the fractions. Finaly, one can also consider inherent properties of low-power HTs, of which the ionization degree is low for low discharge voltage conditions. Thus, the Xe^+ production increases consistently when the voltage is ramped up.
One can also notice that when the discharge voltage is ramped up, the extra peak amplitude increases, in such a way that its amplitude is comparable to the Xe^+ peak for the 350 V case.

Table 7: Ion species fraction recorded on-axis for four different discharge voltages. The ISCT100-v2 was operated with $\dot{m}_a$ = 5 sccm (Xe).

U_d [V]	Xe^+	Xe^{2+}	Xe^{3+}
200	76%	20%	4%
250	85%	14%	1%
300	93%	7%	0%
350	96%	4%	0%

3.3 Effect of the angle

The effect of the angle was also investigated. Measurements were recorded for the probe aligned with the thruster centerline. The ISCT100-v2 was operated with a xenon mass flow rate of 5 sccm and a discharge voltage of 300 V. Measurements were performed for five different angles, namely 0°, 5°, 10°, 15° and 20°, respectively plotted in Figures 7a, 7b, 7c, 7d and 7e. Corresponding ion fractions are given in Table 8.
Peak magnitude clearly depends on the angular position. Xe^+ peak dominates for each angle. As the probe move away from the thruster centerline, the ion current collected is one and two orders of magnitude lower between 0° – 15° and 0° – 20°, respectively. It is worth noticing that at 20°, the signal-to-noise ratio is too low to adequately explore the spectrum. In other words, the ion flux density reaching the collector is too low to discriminate different ion species. This is quite a limiting problem since it does not allow us to fully characterize the far-field plume of the ISCT100-v2 with the actual set-up. When moving away from the thruster centerline, Xe^{2+} and Xe^{3+} peak magnitude increase. This can be explained by the fact that different ion species are created at different locations inside the discharge channel. As a consequence they experience different deflections. Furthermore, the extra peak decreases in intensity and the overlap with the Xe^+ peak is less pronounced for larger angles.

Table 8: Ion species fraction recorded for four different angular positions. The ISCT100-v2 was operated with U_d = 250 V and $\dot{m}_a$ = 5 sccm (Xe).

Angle [°]	Xe^+	Xe^{2+}	Xe^{3+}
0	100%	0%	0%
5	99%	1%	0%
10	81%	18%	1%
15	60%	30%	10%

3.4 Krytpon operation

Krytpon constitutes a good alternative to xenon as gas propellant for HTs. While it presents a higher ionization potential, the lower atomic mass of krypton leads to a larger ion velocity, , hence a higher specific impulse [32, 14]. One would then expect a lower fraction of multiply-charged ions in the plume of a HT operated with krytpon. Indeed, compare to xenon, the energy required to produce doubly- or triply- charged krytpon

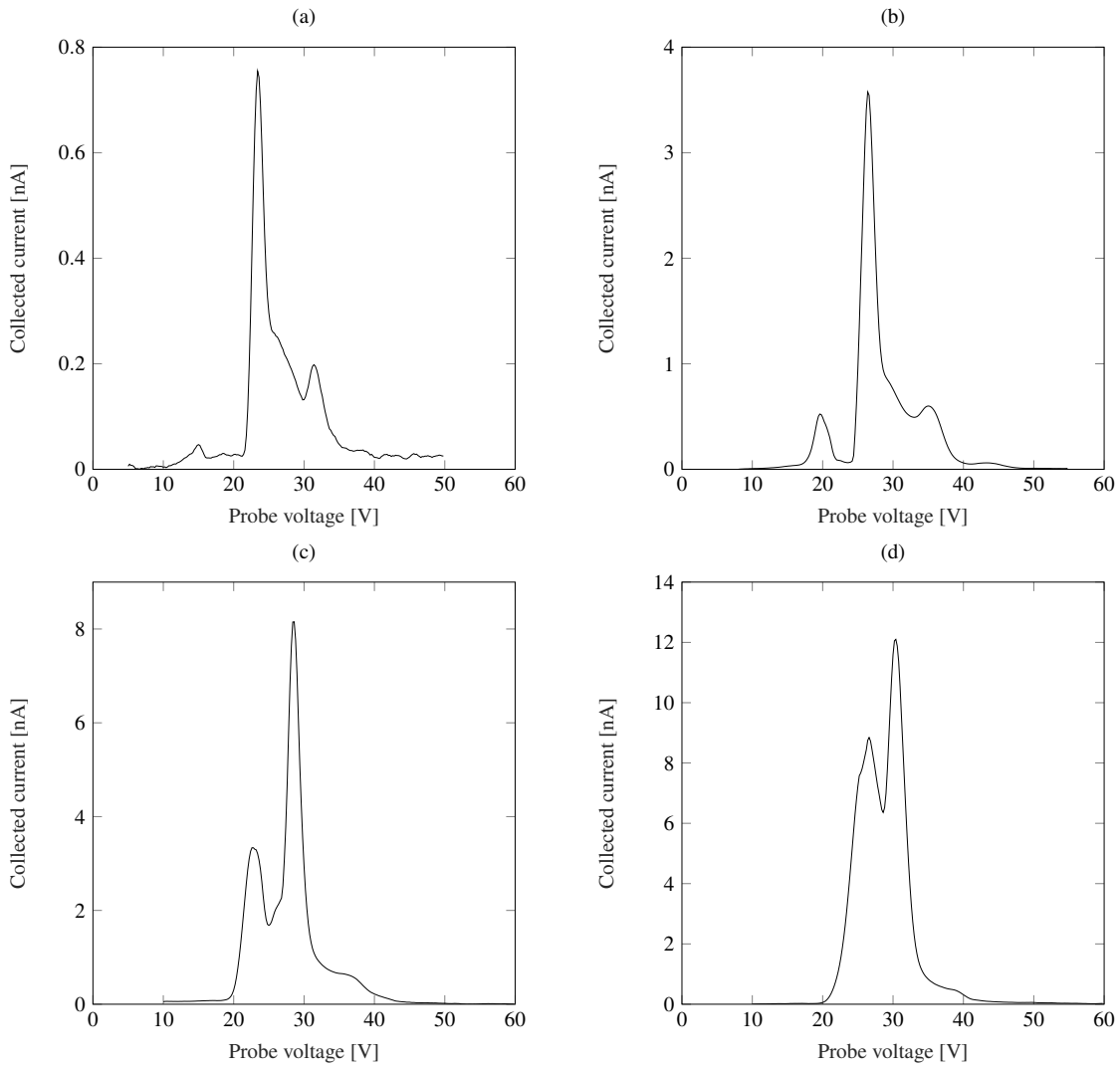

Figure 6: **E**×**B** spectra for $\dot{m}_a$ = 5 sccm of xenon at different discharge voltages, namely **(a)** 200 V, **(b)** 250 V, **(c)** 300 V and **(d)** 350 V. The measurements are recorded for $\theta = 0°$, with the probe aligned with the thruster axis.

ions is much larger than the one needed for xenon. To do so, **E**×**B** measurements were performed in the plume of the 100W-class HT operated with krytpon. Since the magnetic topology and the discharge channel sizes are not optimized for krytpon operation, steady operation were difficult to achieve. The operating parameters investigated are given in Table 2. Note that the krytpon mass flow rate was set in such a way that the discharge power was identic at xenon operations. Figure 8 represents the spectrum recorded for U_d = 300 V and $\dot{m}_a$ = 7.2 sccm, with the probe aligned on the thruster centerline. The spectrum is clairly dominated by singly-charged krytpon ions with a fraction of 98%, while Kr^{2+} only represents 2%. One can also notice that singly- and doubly-charged ions are distinctly separated since the overlapping area between the two species does not exist. In other terms, Kr^{+}–Kr^{2+} elastic collisions are less favoured than Xe^{+}–Xe^{2+}. This observation is physically consistent with the fact that cross section for collisions of krytpon ions are smaller than xenon ones at a given electron energy [33]. The extra peak is still visible but it exhibits a lower magnitude.

Furthermore, krytpon ion velocities are higher than xenon ones. The Kr^{+} and Kr^{2+} peaks are respectively associated to probe voltages of 34.4 V and 48.8 V, which corresponds to uncorrected velocities of 24.571 km.s^{-1} and 34.857 km.s^{-1}. Such observation is not surprising since it is due to the lower atomic mass of krypton. As expected, the ratio between $v_{ion}(Kr^{+})$ and $v_{ion}(Kr^{2+})$ is $\sqrt{2}$.

4 Conclusion

In this study, we have estimated ion species fractions and measured the corresponding velocities in the far-field plume of the 100 W-class ISCT100-v2 HT, by means of an **E**×**B** porbe. After having studied the influence of the probe alignment on the spectra shape, the impact of background pressure, discharge voltage and angular position has been inves-

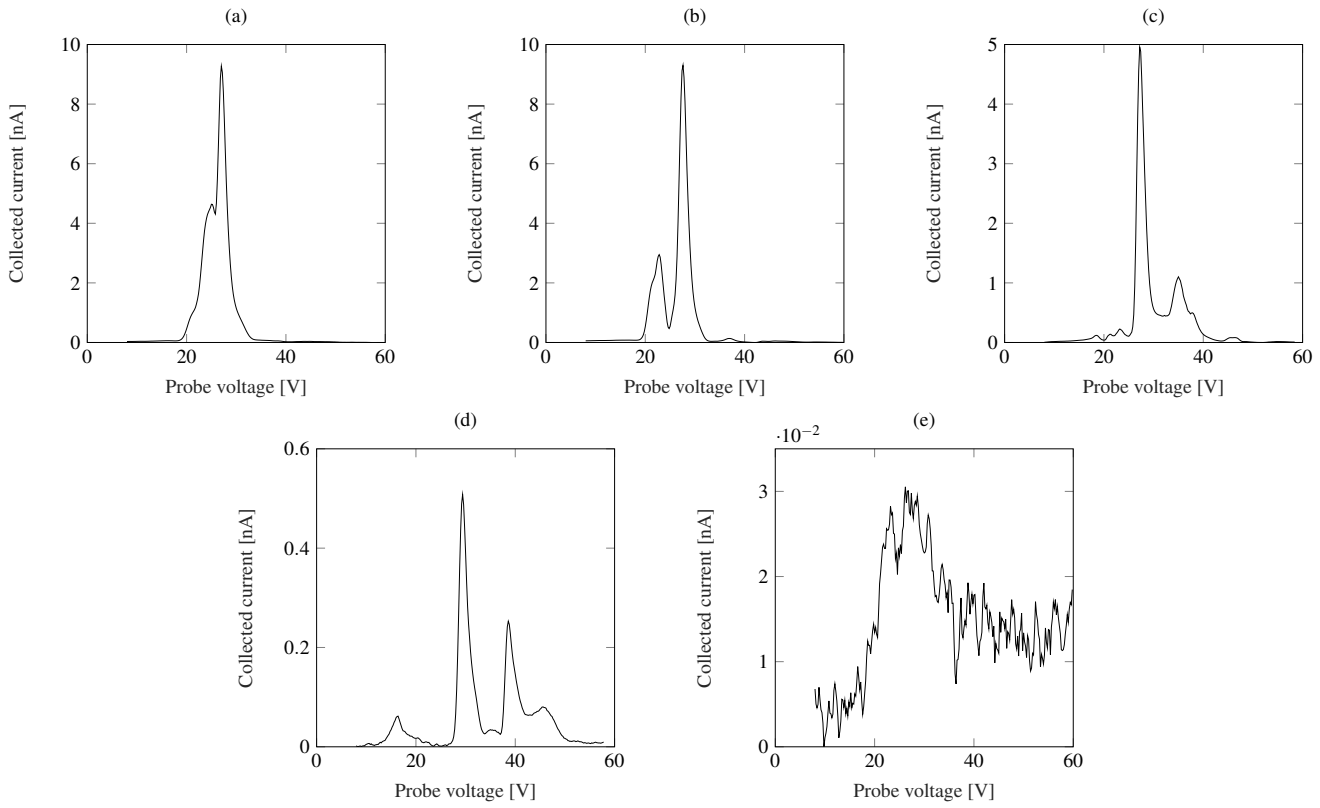

Figure 7: **E**×**B** spectra for U_d = 300 V and $\dot{m}_a$ = 5 sccm at different angular positions, namely **(a)** $\theta = 0°$, **(b)** $\theta = 5°$, **(c)** $\theta = 10°$, **(d)** $\theta = 15°$, **(e)** $\theta = 20°$. The measurements are recorded with the probe aligned with the thruster axis.

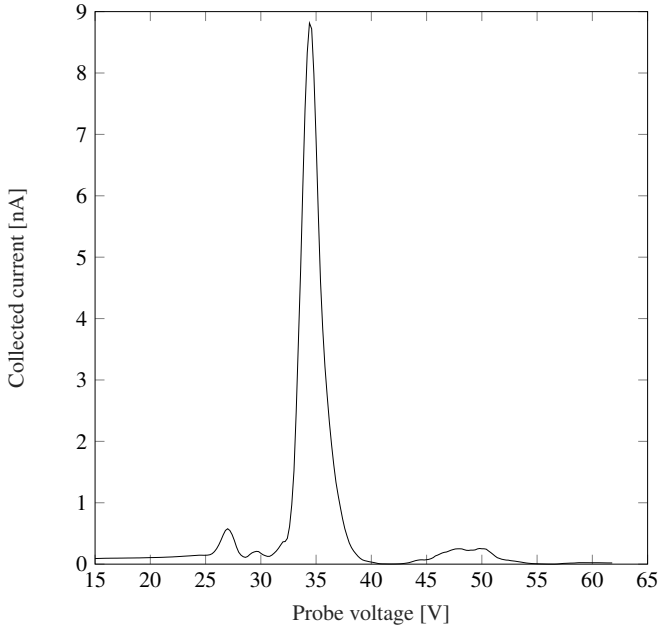

Figure 8: **E**×**B** spectra for U_d = 300 V and $\dot{m}_a$ = 7.2 sccm (Kr) at $\theta = 0°$. The measurements are recorded with the probe aligned with the thruster centerline.

tigated for the thruster operated with both xenon and krypton. One unexpected result is that the fraction of the multiply charged ions does not increase with the discharge voltage on the thruster centerline, compare to what was described for mid- and high-power class HTs. This fraction increases as the probe is moved away from the thruster centerline however. A 180° plume characterization at various discharge voltages must be performed to confirm the observed results.

The study also points out some limits of the **E**×**B** probe design for low power, i.e. low-current, electric propulsion devices, since the measurements are only usable in a small portion of the plume, namely for $-15° < \theta < 15°$, where the ion flux is the highest. Such a problem is quite challenging since it is due to the inherent properties of low-power HTs.

To complete this study and gain insight into ion plume properties, Laser Induced Fluorescence spectroscopy will be performed in an upcoming experimental campaign.

References

[1] Richard R. Hofer and Robert S. Jankovsky. A hall thruster performance model incorporating the effects of a multiply-charged plasma. In *37th AIAA/ASME/SAE/ASEE Joint Propulsion Conference and Exhibit, Salt Lake City, Utah, July 8-11*, number 2001-3322, pages 1–17, 2001.

[2] Alec D. Gallimore. Near- and Far-Field Characterization of Stationary Plasma Thruster Plumes Introduction. *Journal of spacecraft and rockets*, 38(3):441–453, 2001.

[3] T. Randolph, E. Pencil, and D. Manzella. Far-field plume contamination and sputtering of the stationary plasma thruster. In *30th AIAA/ASME/SAE/ASEE Joint Propulsion Conference, Indianapolis, June 27-29, 1994*, 1994.

[4] Lyon B. King and Alec D. Gallimore. Ion Energy Diagnostics in the Plume of an SPT-100 from Thrust Axis to Backflow Region. *AIAA*, 1998.

[5] Yassir Azziz, Manuel Martinez-Sanchez, and James J. Szabo. Effect of Discharge Voltage on Plume Divergence of a High Specific Impulse Hall Thruster. In *41st AIAA/ASME/SAE/ASEE Joint Propulsion Conference and Exhibit, Tucson, Arizona, The United States of America, July 10-13*, number 2005-4403, pages 1–14, 2005.

[6] Kevin D. Diamant, Raymond Liang, and Ronald L. Corey. The Effect of Background Pressure on SPT-100 Hall Thruster Performance. In *50th AIAA/ASME/SAE/ASEE Joint Propulsion Conference and Exhibit, Cleveland, Ohio, The United States of America, July 28-30*, number 2014-3710, pages 1–17, 2014.

[7] Frank S. Gulczinski and Alec D. Gallimore. Near-Field Ion Energy and Species Measurements of a 5-kW Hall Thruster Introduction. *Journal of Propulsion and Power*, 17(2):418–427, 2001.

[8] Ian H. Hutchinson. *Principles of Plasma Diagnostics*. Cambridge University Press, Cambridge, UK, second edi edition, 2002.

[9] Lyon B. King. *Transport-Property and Mass Spectral Measurements in the Plasma Exhaust Plume of a Hall Effect Space Propulsion System*. PhD thesis, 1998.

[10] Sang-Wook Kim. *Experimental investigations of plasma parameters and species-dependent ion energy distribution in the plasma exhaust plume of a Hall thruster*. PhD thesis, The University of Michigan, 1999.

[11] Thibault Hallouin, Stéphane Mazouffre, M. Inchingolo, Antonio Gurciullo, Paul Lascombes, and Jean-Luc Maria. Far-field plume diagnostic of the 100 W-class ISCT100-v2 Hall thruster. In *36th International Electric Propulsion Conference, University of Vienna, Austria, September 15-20*, number 2019-617, pages 1–32, 2019.

[12] Thibault Hallouin and Stéphane Mazouffre. Far-field plume characterization of a 100-W class Hall thruster. *Aerospace*, 58(7):1–21, 2020.

[13] Richard R. Hofer and Alec D. Gallimore. Ion Species Fractions in the Far-Field Plume of a High-Specific Impulse Hall Thruster. In *39th AIAA/ASME/SAE/ASEE Joint Propulsion Conference and Exhibit, Huntsville, Alabama, The United States of America, July 20-23*, number 2003-5001, pages 1–16, Huntsville, Alabama, USA, 2003. National Aeronautics and Space Administration.

[14] Richard R. Hofer and Alec D. Gallimore. High-Specific Impulse Hall Thrusters , Part 2 : Efficiency Analysis. *Journal of Propulsion and Power*, 22(4):732–740, 2006.

[15] Jared M. Ekholm and William A. Hargus. E x B Measurements of a 200 W Xenon Hall Thruster. In *34th AIAA/ASME/SAE/ASEE Joint Propulsion Conference and Exhibit, Cleveland, Ohio, The United States of America, July 13-15*, number 2005-4405, pages 1–9, 2005.

[16] Jared M. Ekholm, William A. Hargus, C. William Larson, Michael R. Nakles, Garrett Reed, and Carrie S. Niemela. Plume Characteristics of the BHT-HD-600 Hall Thruster. Technical report, Air Force Research Laboratory, 2006.

[17] Bryan M. Reid, Rohit Shastry, Alec D. Gallimore, and Richard R. Hofer. Angularly-Resolved ExB Probe Spectra in the Plume of a 6-kW Hall Thruster. In *44th AIAA/ASME/SAE/ASEE Joint Propulsion Conference and Exhibit, Hartford, Connecticut, The United States of America, July 21-23*, number 2008-5287, pages 1–21, 2008.

[18] Kevin D. Diamant, Rostislav Spektor, Edward J. Beiting, Jason A. Young, and Thomas J. Curtiss. The Effects of Background Pressure on Hall Thruster Operation. In *48th AIAA/ASME/SAE/ASEE Joint Propulsion Conference and Exhibit, Atlanta, Georgia, The United States of America, July 30 - August 01*, number 2012-3735, pages 1–13, 2012.

[19] Kevin D. Diamant, Thomas J. Curtiss, Rostislav Spektor, Edward J. Beiting, Vlad Hruby, Bruce Pote, Juraj Kolencik, and Surjeet Paintal. Performance and Plume Characterization of the BHT-1500 Hall Thruster. In *34th International Electric Propulsion Conference, Hyogo-Kobe, Japan, July 4-10*, number 2015-69, pages 1–16, 2015.

[20] Kevin D. Diamant, Ty Lee, Raymond Liang, Jonathan Noland, Vanessa Vial, and Nicolas Cornu. Performance and Plume Characterization of the PPS ® 1350-G Hall Thruster. In *52nd AIAA/SAE/ASEE Joint Propulsion Conference and Exhibit, Salt Lake City, Utah, The United States of America, July 25-27*, number 2016-4543, pages 1–16, 2016.

[21] Antonio Gurciullo, Andrea Lucca Fabris, and Mark A. Cappelli. Ion plume investigation of a Hall effect

thruster operating with Xe/N2 and Xe/air mixtures. *Journal of Physics D: Applied Physics*, 52(46), 2019.

[22] Hiroki Watanabe, Shinatora Cho, and Kenichi Kubota. Performance Evaluation of a 100-W Class Hall Thruster. In *36th International Electric Propulsion Conference, University of Vienna, Austria, September 15-20*, number 2019-447, pages 1–13, 2019.

[23] James J. Szabo, Rachel Tedrake, Emily Metivier, Surjeet Paintal, and Zachary Taillefer. Characterization of a One Hundred Watt, Long Lifetime Hall Effect Thruster for Small Spacecraft. In *53rd AIAA/SAE/ASEE Joint Propulsion Conference and Exhibit, Atlanta, Georgia, The United States of America, July 10-12*, number 2017-4728, 2017.

[24] Stéphane Mazouffre and Lou Grimaud. Characteristics and Performances of a 100-W Hall Thruster for Microspacecraft. *IEEE Transactions on Plasma Science*, 46(2):330–337, 2018.

[25] Denis Renaud, D. Gerst, Stéphane Mazouffre, and A. Aanesland. E x B probe measurements in molecular and electronegative plasmas. *Review of Scientific Instruments*, 86(12), 2015.

[26] Julien Vaudolon. *Electric field determination and magnetic topology optimization in Hall thrusters*. PhD thesis, Université d'Orléans, 2015.

[27] Sang-Wook Kim and Alec D. Gallimore. Plume study of a 1.35-kW SPT-100 using a ExB probe. *Journal of Spacecraft and Rockets*, 39(6):904–909, 2002.

[28] Richard R. Hofer. Development and characterization of high-efficiency , high-specific impulse xenon Hall thrusters. 2004.

[29] Wensheng Huang and Rohit Shastry. Analysis of Wien filter spectra from Hall thruster plumes. *Review of Scientific Instruments*, 86(7):1–11, 2015.

[30] Rohit Shastry, Richard R. Hofer, Bryan M. Reid, and Alec D. Gallimore. Method for analyzing E×B probe spectra from Hall thruster plumes. *Review of Scientific Instruments*, 80(6), 2009.

[31] D. Gawron, Stéphane Mazouffre, N. Sadeghi, and A. Héron. Influence of magnetic field and discharge voltage on the acceleration layer features in a Hall effect thruster. *Plasma Sources Science and Technology*, 17(2):2–12, 2008.

[32] Jesse A. Linnell and Alec D. Gallimore. Efficiency analysis of a Hall thruster operating with krypton and xenon. *Journal of Propulsion and Power*, 22(6):1402–1412, 2006.

[33] Jack A Syage. Electron-impact cross sections for multiple ionization of Kr and Xe. *PHYSICAL REVIEW A*, 46(9):5666–5679, 1992.